Thermal convection of liquid metal in a long inclined cylinder

Andrei Teimurazov* and Peter Frick
Institute of Continuous Media Mechanics, 1 Akademika Koroleva Street, Perm 614013, Russia
(Received 7 August 2017; published 2 November 2017)

The turbulent convection of low-Prandtl-number fluids ($\mathrm{Pr} = 0.0083$) in a long cylindrical cell, heated at one end face and cooled at the other, inclined to the vertical at angle β, $0 \leqslant \beta \leqslant \pi/2$ with step $\pi/20$, is studied numerically by solving the Oberbeck-Boussinesq equations with the large-eddy-simulation approach for small-scale turbulence. The cylinder length is $L = 5D$, where D is the diameter. The Rayleigh number, determined by the cylinder diameter, is of the order of 5×10^6. We show that the structure of the flow strongly depends on the inclination angle. A stable large-scale circulation (LSC) slightly disturbed by small-scale turbulence exists in the horizontal cylinder. The deviation from a horizontal position provides strong amplification of both LSC and small-scale turbulence. The energy of turbulent pulsations increases monotonically with decreasing inclination angle β, matching the energy of the LSC at $\beta \approx \pi/5$. The intensity of the LSC has a wide, almost flat, maximum for an inclined cylinder and slumps approaching the vertical position, in which the LSC vanishes. The dependence of the Nusselt number on the inclination angle has a maximum at $\beta \approx 7\pi/20$ and generally follows the dependence of the intensity of LSC on the inclination. This indicates that the total heat transport is highly determined by LSC. We examine the applicability of idealized thermal boundary conditions (BCs) for modeling a real experiment with liquid sodium flows. Therefore, the simulations are done with two types of temperature BCs: fixed face temperature and fixed heat flux. The intensity of the LSC is slightly higher in the latter case and leads to a corresponding increase of the Nusselt number and enhancement of temperature pulsations.

DOI: 10.1103/PhysRevFluids.2.113501

I. INTRODUCTION

Heat transport in turbulent convective flow has been widely studied for the classical model of Rayleigh-Bénard convection (RBC), i.e., convection in a horizontal layer or confined domain with characteristic aspect ratio $D/L \gtrsim 1$. Here L is the vertical dimension and D is the characteristic horizontal dimension, e.g., the diameter of a cylindrical domain. The effective heat transport, characterized by the Nusselt number Nu, is determined by the Rayleigh number $\mathrm{Ra}_L = \alpha g \Theta L^3/\nu\chi$ and Prandtl number $\mathrm{Pr} = \nu/\chi$. Here α is the thermal expansion coefficient, ν is the kinematic viscosity, χ is the thermal diffusivity of the fluid, g is the gravity acceleration, and $\Theta = T^+ - T^-$ is the temperature difference between the hot (T^+) and the cold (T^-) isothermal boundaries. However, even for the RBC case under a large or moderate aspect ratio Γ, the dependence $\mathrm{Nu} \sim \mathrm{Ra}^\eta \mathrm{Pr}^\zeta$ exhibits on the Ra-Pr plane a variety of regimes with different values of η and ζ [1–4].

Tilting of the convective cell influences the structure of the flow and the heat transport. Many studies, made for fluids with $\mathrm{Pr} > 1$, reveal a weak reduction of the Nusselt number under small inclination angle β [5–8]. Here and below, $\beta = 0$ corresponds to RBC and $\beta = \pi/2$ corresponds to the case of horizontal cylinder with vertical heaters. Recently, direct numerical simulations of convection in a cell with $L = D$ showed that a small inclination decreases the Nusselt number for liquids with $\mathrm{Pr} = 100$ and 10, but increases for liquids with $\mathrm{Pr} = 1$ and 0.1 [9]. A weak increase of Nu for very small inclination angles, followed by a decrease, was also found at $\mathrm{Pr} = 4.4$ and $L/D = 0.5$ [8].

*tas@icmm.ru

In long cylinders (pipes), the dependence on inclination angle becomes more complicated. Experiments with long tubes ($10 < L/D < 50$) filled with liquid helium demonstrated that an inclination leads to a strong increase of the Nusselt number with a maximum at inclination angle $\beta \approx 70^\circ$ [10]. An increase in the efficiency of heat transfer with increasing inclination from $\beta = 0$ to $\beta = 45^\circ$ was also observed in an experimental study of turbulent convection in a channel connecting two reservoirs with hot and cold water [11].

Recently, the problem of turbulent convective heat transfer in long tubes having three different orientations with respect to gravity (vertical, horizontal, and inclined at 45°) has been examined experimentally for a liquid metal (sodium) [12,13]. It was shown that convective heat transfer in cylinders with $L \gg D$ under moderate Rayleigh number is mainly provided by the large-scale sodium circulation and is most effective in an inclined cylinder, in which a strong circulation develops on a background of developed turbulence. In the long cylinder ($L = 20D$), at $\mathrm{Ra}_D \approx 10^6$ (the Rayleigh number was defined through the diameter of the cylinder), the Nusselt number reached a maximum at inclination about 65° to the vertical and was three times higher than in the horizontal cylinder and about ten times higher than in the vertical one [14].

Peculiarity of convection in liquids with small Prandtl numbers is provided by large ratio of the thickness of the thermal to kinetic boundary layers (BLs) (thick thermal BLs and thin kinetic BLs). Then, for the RBC, two basic regimes can be established [3]. If the upper and lower thermal BLs merge (cells with small vertical dimension and moderate Rayleigh numbers), the regime II_l is observed (following the Grossmann-Lohse classification; see [3] for details). Then the thermal energy is mainly dissipated in BLs, while the kinetic energy is mainly dissipated in the turbulent bulk. The Nusselt number depends on the Rayleigh number and Prandtl number as $\mathrm{Nu} \sim (\mathrm{RaPr})^{1/5}$. In cells with a large vertical dimension under strong heating (large Rayleigh numbers), the thermal BLs are distended and both the kinetic and thermal energies are mainly dissipated in the bulk. This is the regime IV_l, characterized by the power law $\mathrm{Nu} \sim (\mathrm{RaPr})^{1/2}$. Experiments with convection of liquid sodium in long vertical cylinders show that the power exponent increases with increasing ratio L/D: $\mathrm{Nu} \sim (\mathrm{RaPr})^{0.6}$ was observed in a cylinder with length $L = 5D$ [12] and $\mathrm{Nu} \sim (\mathrm{RaPr})^{0.84}$ in a cylinder with $L = 20D$ [13]. Note that these values exceed the upper bound for power exponent ($\mathrm{Nu} \sim \mathrm{Ra}^{1/2}$), known from variational analysis for classical Oberbeck-Boussinesq Rayleigh-Bénard convection [15], which, however, did not consider narrow vertical tubes.

The structure of boundary layers in high-Rayleigh-number convection under small Prandtl number becomes of special interest. Recently, very-high-resolution numerical simulations allowed the study of the dynamics of boundary layers in liquid metal RBC in a wide range of Rayleigh numbers ($10^5 < \mathrm{Ra} < 5\times10^8$ and $L = D$) [16]. More and more detailed numerical simulations for liquid metal turbulent convection in confined cells with isothermal boundary conditions (BCs) have been performed (i.e., [9,17]). It is worth noting that experimentally it is impossible to realize perfect isothermal BCs for low-Prandtl-number fluids (liquid metals) whose thermal diffusivity is close to the diffusivity of the best available wall materials. This causes the problem of satisfying and matching BCs between experiments and numerical simulations.

The aim of this paper is twofold. First, we intend to reproduce in numerical simulations the results of a specific experiment on turbulent convection in a liquid metal. In particular, we examine the applicability of idealized thermal BCs for modeling real low-Prandtl-number flows and the capability of relatively low-resolution large-eddy simulations (LES) for reproducing peculiarity of heat transfer in turbulent convective flows. Second, we study the flow structure and the effective heat transfer under turbulent convection in an elongated cylinder ($L = 5D$) inclined to the vertical at angle $0 \leqslant \beta \leqslant \pi/2$.

II. EXPERIMENTAL PROTOTYPE AND NUMERICAL MODEL

Our simulations are intended to reproduce the convective flow in a real experimental setup to recover in simulations the flow characteristics, which are unattainable in laboratory experiments. Thus, we try to approximate the actual parameters of the setup used in laboratory experiments [12,18].

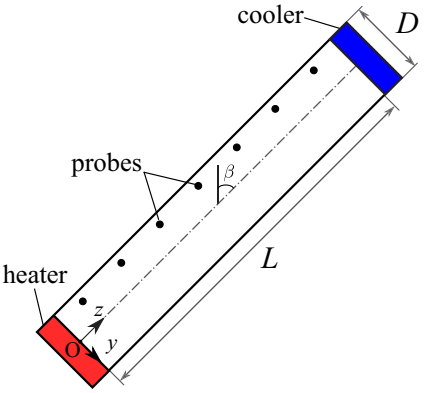

FIG. 1. Convective cell with the coordinate system and the probe locations where experimental data are available.

In these experiments, the convection of sodium was studied in a cylinder of length $L = 850$ mm and diameter $D = 168$ mm made from stainless steel (the wall thickness was 6 mm). Our computational domain is a cylinder with exactly the same dimensions, so $L \simeq 5D$.

In the experiments, the cylinder was closed by copper heat exchangers (see Fig. 1). The end heater consisted of four 15-mm copper plates with electrical heaters located in grooves. The sodium-oil heat exchanger (the cooler) consisted of two copper plates, cooled by mineral oil, circulating in the labyrinth groove. The total heat loss through the cylinder insulation was estimated to be below 13% of the heater power. Temperature measurements were made by seven thermocouples (shown in Fig. 1) located along the cylinder's generatrix at a distance of 17 mm from the wall, 119 mm apart. These thermocouples were also used to estimate the average axial velocity component in the area between adjacent probes. Additional thermocouples were arranged within the copper plates and in the sodium near the plates. The setup design allowed the heaters' temperature and coolant flow rate to be set. Then, for a specified heater temperature and coolant flow rate, a steady convection regime was achieved and the measurements were carried out. The temperature difference between the end heat exchangers reached 30 °C, but the mean temperature of the sodium at different regimes varied greatly, from 130 °C to 240 °C. In this temperature range, the sodium Prandtl number varies from 0.0094 to 0.0064. In simulations, we have chosen regimes with the mean temperature of the sodium about 165 °C with corresponding Prandtl number $\mathrm{Pr} = 0.0083$.

The numerical code solves the Oberbeck-Boussinesq equations of thermogravitational convection. We use the LES approach for modeling turbulence, namely, the Smagorinsky-Lilly model [19,20] with the Smagorinsky constant $C_s = 0.14$ and turbulent Prandtl number $\mathrm{Pr}_t = 0.9$. Simulations were carried with a numerical grid consisting of 1.65×10^6 nodes. To resolve the boundary layers, a nonuniform numerical grid with a higher density of points near the boundaries was used. The sufficient number of grid points in the boundary layer depends on large-scale circulation (LSC) and Ra number [21–23]; boundary layers in low Pr convection are highly transitional [16]. Figure 2 demonstrates the temperature and velocity profiles along the cylinder axis in the boundary layer under a fixed axial heat flux for inclination angle $\beta = \pi/4$. In the case of low Pr numbers the velocity BL is very thin (for the case considered the thickness is approximately equal to 2.2 mm) and the figure shows that the number of grid points in the BL is not less than 5. The terms with time derivatives are discretized using an implicit Euler scheme. The convective terms are computed by the limited linear total variation diminishing scheme [24]. All the simulations were run using the finite volume code OpenFOAM-extend 3.2 [25]. The numerical simulations were performed on the supercomputer Triton of ICMM UB RAS.

It is hard to reproduce the real BCs in simulations. The thermal conductivity of copper is only about four times higher than the conductivity of sodium. Measurement inside inner copper plates

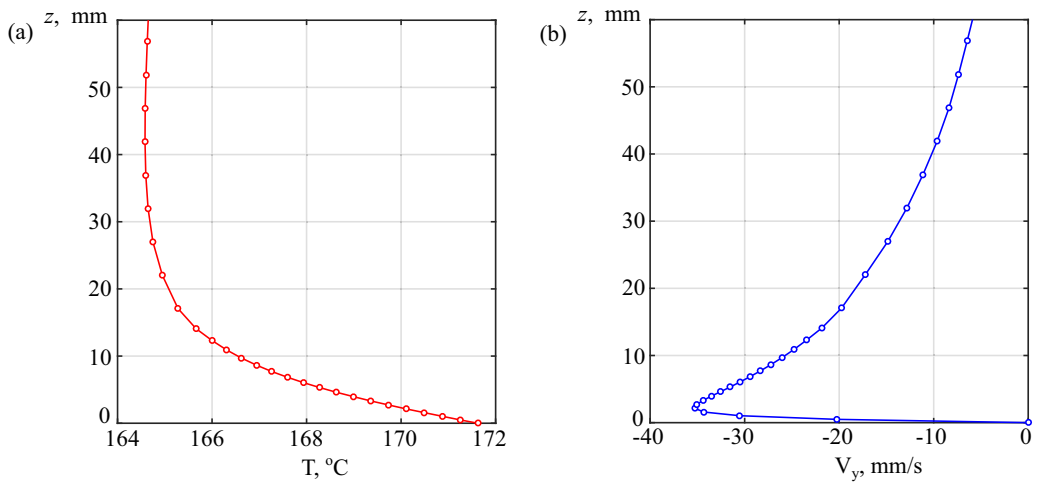

FIG. 2. (a) Time-averaged temperature profile and (b) velocity component V_y profile along the cylinder axis in the boundary layer under a fixed axial heat flux for inclination angle $\beta = \pi/4$. Circles correspond to the nodes of a numerical grid. The temperature BL for this case has thickness approximately equal to 32 mm and the velocity BL has thickness approximately equal to 2.2 mm.

detected essential temperature differences, up to 6 °–7 °C, while the applied mean temperature difference between the ends of the inclined cylinder was about 20 °C [18]. Because the heat flux was actually fixed in the experiments, we have chosen the problem with fixed heat flux for the basic configuration of our simulations. Thus, we start by considering the sodium convection in the cylinder under fixed heat power $Q = 1314$ W (the heat flux is $q = 59.3$ kW/m^2). Actually, this is the heat output provided by the cooling system in the experiments. The influence of the thermal BCs on the end faces of the cylinder will be discussed in Sec. IV. The sidewalls are heat insulated. The no-slip velocity conditions are applied at all boundaries.

III. SODIUM FLOW IN VERTICAL, INCLINED, AND HORIZONTAL CYLINDERS WITH FIXED AXIAL HEAT FLUX

First, we analyze the general structure of the turbulent convective flow that develops in the cylinder under fixed heat flux at three basic positions: vertical ($\beta = 0$), inclined at $\beta = \pi/4$ to the vertical, and horizontal ($\beta = \pi/2$). The heat flux in all positions is $q = 59.3$ kW/m^2. The Rayleigh number $\mathrm{Ra}_D = \alpha g \Theta D^3/\nu\chi$, defined through the diameter and the mean temperature difference between the faces, varies slightly with inclination and is in the range $\mathrm{Ra}_D = (4.8{-}7.7){\times}10^6$. All statistics are performed over a time interval of the order of 1 h, corresponding to more than 1500 dimensionless time units, defined as $(D/g\alpha\Theta)^{1/2}$.

The mean velocity fields for these positions are shown in Fig. 3. In the vertical cylinder, no mean flow is seen in the bulk of the cylinder. Only two stable ring vortices exist near both end faces [Fig. 3(a)]. In the inclined cylinder, a very pronounced LSC appears against the turbulent background. In practice, this LSC covers the whole cavity. At $\beta = \pi/4$, only two weak counterrotating vortices survive in the topmost and bottommost cylinder parts [Fig. 3(b)]. No counterrotating vortices are seen in the mean flow in the horizontal cylinder. In the inclined cylinder, the LSC is much stronger in comparison to the horizontal cylinder and the maximum flow velocity is much higher (0.073 versus 0.047 m/s). In the experiments, the velocity estimations were done by cross-correlation analysis of temperature oscillations: Maximal values were obtained from the two thermocouples nearest the heater and gave 0.060 m/s for $\beta = \pi/4$ and 0.039 m/s for $\beta = \pi/2$ [18]. These values are in good

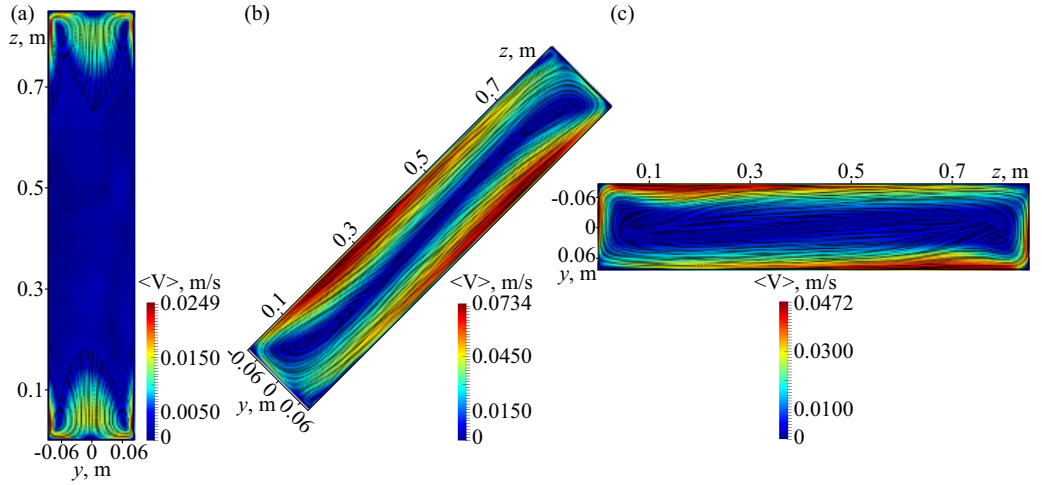

FIG. 3. Time-averaged velocity fields in the yOz plane under a fixed axial heat flux for inclination angle (a) $\beta = 0$, (b) $\beta = \pi/4$, and (c) $\beta = \pi/2$. Field visualization by line integral convolution technique; the magnitudes of velocity are shown by color.

agreement with values obtained at the same positions in our simulations: 0.056 m/s for $\beta = \pi/4$ and 0.035 m/s for $\beta = \pi/2$.

The intensity of turbulence can be characterized by the distribution of the energy of turbulent pulsations or by the standard deviation (SD). Figure 4 shows the velocity SD fields for three cases. The most developed turbulence is observed in the vertical cylinder. The intense small-scale turbulence occupies the whole cylinder and is most intense along the sidewalls [Fig. 4(a)]. In the inclined cylinder, the total intensity of turbulence decreases and its distribution differs. The most intense pulsations are provided by interacting ascending and descending large-scale flows and they occupy the central part of the cylinder [Fig. 4(b)]. In the horizontal cylinder, the overall pulsations field is much weaker in comparison to the previous cases [Fig. 4(c)]. The pulsations are concentrated in very small "corners" and no real turbulence exists in the bulk.

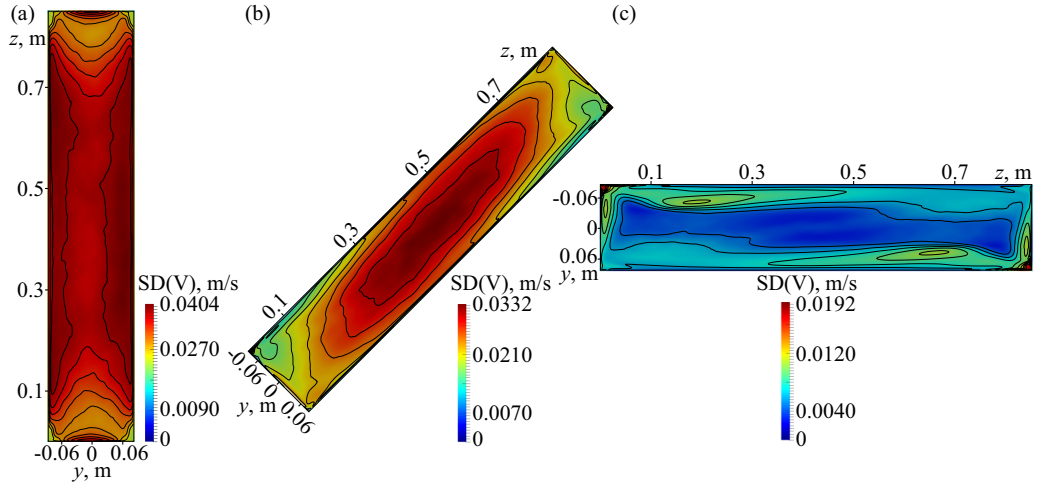

FIG. 4. Standard deviation of velocity fields in the yOz plane for (a) $\beta = 0$, (b) $\beta = \pi/4$, and (c) $\beta = \pi/2$.

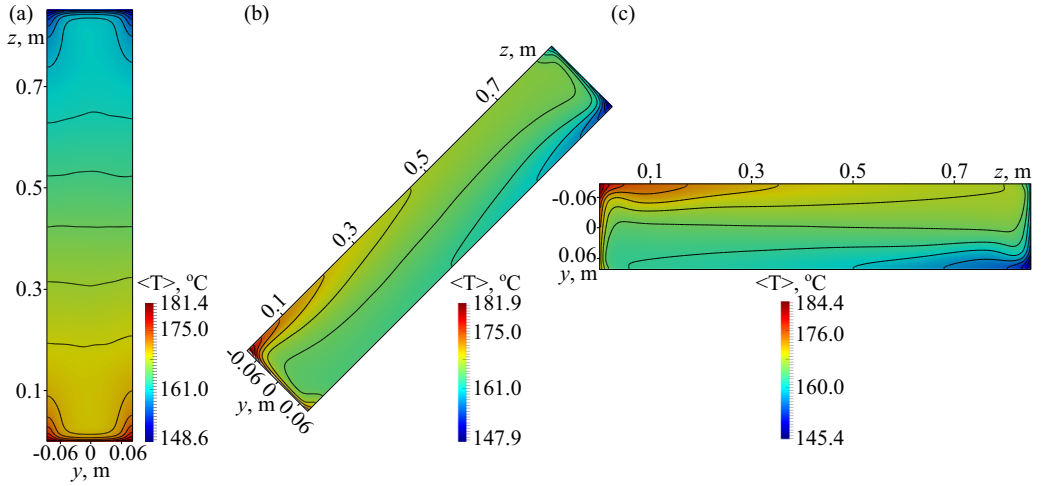

FIG. 5. Time-averaged temperature fields in the yOz plane for (a) $\beta = 0$, (b) $\beta = \pi/4$, and (c) $\beta = \pi/2$.

Thus, in the vertical cylinder LSC is absent, but the energy of turbulent fluctuations is maximal. In the inclined cylinder, the strong LSC develops on a background of developed turbulence. In the horizontal cylinder, LSC is less intense, turbulent fluctuations are small, and the flow can be characterized as transient to turbulent.

The structure of the mean temperature fields is shown in Fig. 5. In the vertical cylinder, the homogeneous vertical temperature gradient dominates in the bulk of the cylinder. Two ring vortices provide a pronounced radial temperature gradient in the lower and upper domains of the cylinder [Fig. 5(a)]. In the inclined and horizontal cylinders, the mean temperature field is determined by the LSC, which carries up the hot fluid along the upper sidewall and carries down the cold fluid along the lower sidewall [Figs. 5(b) and 5(c)].

Figure 6 shows the corresponding SD fields for the temperature. At all cylinder positions, the temperature pulsations are concentrated near the heat exchangers and are entrained to some extent

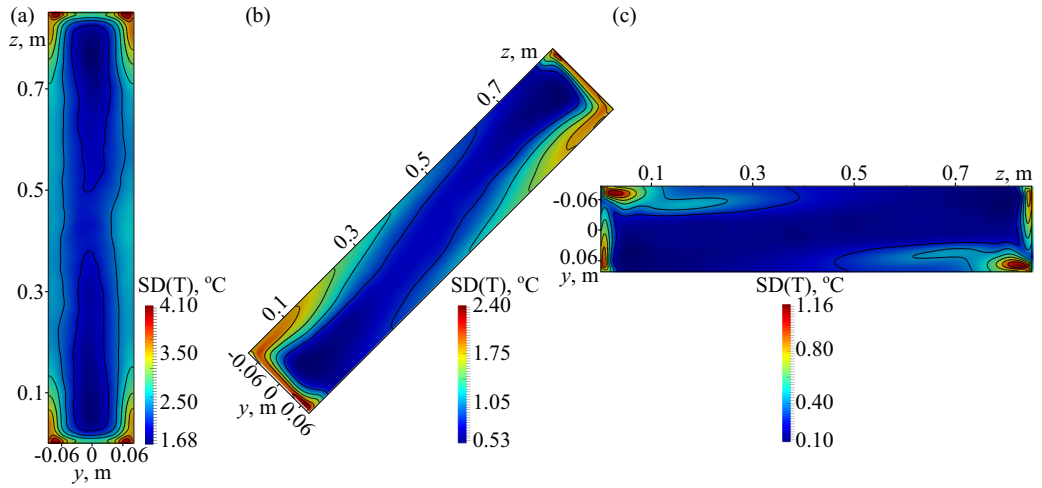

FIG. 6. Standard deviation of temperature fields in the yOz plane for (a) $\beta = 0$, (b) $\beta = \pi/4$, and (c) $\beta = \pi/2$.

by the adjacent flows (by ring vortices in the vertical cylinder and by LSC in the inclined cylinder). The strongest pulsations occur in the vertical cylinder [Fig. 6(a)]. The temperature pulsations at $\beta = \pi/4$ [Fig. 6(b)] are considerably lower than at $\beta = 0$. In the horizontal position ($\beta = \pi/2$), the fluid flow is most stable and the temperature pulsations are weakest [Fig. 6(c)].

IV. IMPACT OF END FACE THERMAL BOUNDARY CONDITIONS

Standard thermal BCs for RBC imply that there is a fixed temperature at the horizontal boundaries. Thus, first type (Dirichlet) of thermal BCs is mainly used in numerical simulations of RBC. We will refer to them as BC I, in contrast to the second type (Neumann), BC II. In experiments, to provide a constant temperature at the heated and cooled surfaces, massive copper heat exchangers are used. For liquid metals, the preference for copper heat exchangers diminishes. For gallium and mercury, which are mainly used for convective experiments, the thermal diffusivity is an order of magnitude below the thermal diffusivity of copper. The thermal diffusivity of sodium is only about 1.5 times less than the diffusivity of copper, so the ratio of thermal conductivities is about 4.5. Therefore, the temperature distribution on the faces in sodium experiments is nonuniform and it is difficult to measure the actual temperature field on the face end.

Because we cannot reproduce the actual experimental BCs, we analyze the impact of the BCs in numerical simulations. First, we restore the time-averaged temperature distribution on the face end, established under a fixed homogeneous heat flux (i.e., BC II). Figure 7 shows the averaged temperature field at the bottom plate for inclination angles $\beta = 0, \pi/4$, and $\pi/2$ obtained in numerical simulations with fixed heat flux $q = 59.3$ kW/m^2. Actually, the heterogeneity is significant in all three cases. In the vertical cylinder, the distribution is axisymmetric with a lower temperature in the central area [Fig. 7(a)]. In the inclined and horizontal cylinders, the temperature field at the bottom is determined by the LSC flow, which washes the face from the bottom up by cold liquid [Figs. 7(b) and 7(c)]. The largest temperature difference on the bottom plate is observed in the horizontal cylinder.

Second, we perform numerical simulations with BC I, fixing the temperature on the face ends. The temperature of each face was taken as equal to the mean temperature over the same face calculated in a previous simulation for the same cylinder inclination, but with BC II, i.e., with fixed heat flux. The calculated average temperature difference Θ between two faces was $\Theta = 27.66\,^\circ$C for $\beta = 0$, $\Theta = 18.18\,^\circ$C for $\beta = \pi/4$, and $\Theta = 19.60\,^\circ$C for $\beta = \pi/2$. The minimal value $\Theta = 17.39\,^\circ$C was observed at $\beta = 7\pi/20$. Note that for simulations with BC II the Rayleigh number Ra_q defined through the heat flux is often used [26,27]. We prefer to use the Rayleigh number defined through Θ for both BCs because it simplifies the comparison of results. It is clear that under fixed heat flux Ra_q is constant for any inclination angle, but Ra changes: The maximal $\mathrm{Ra} = 7.7\times10^6$ corresponds to the vertical position and the minimal $\mathrm{Ra} = 4.8\times10^6$ corresponds to $\beta = 7\pi/20$.

We do not show the averaged and SD fields of velocity and temperature, obtained in simulations with BC I, because they are all so similar to the corresponding fields in Figs. 3–6 that the difference is not visible to an unaided eye. The structure of the velocity and temperature fields of the bulk flow weakly depends on the end face thermal BC. To demonstrate the difference between fixed

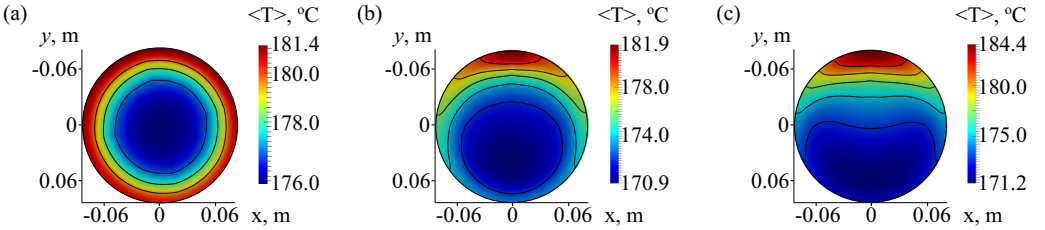

FIG. 7. Time-averaged temperature fields in the xOy plane at $z = 0$ (the heated surface) in simulations with fixed heat flux for (a) $\beta = 0$, (b) $\beta = \pi/4$, and (c) $\beta = \pi/2$.

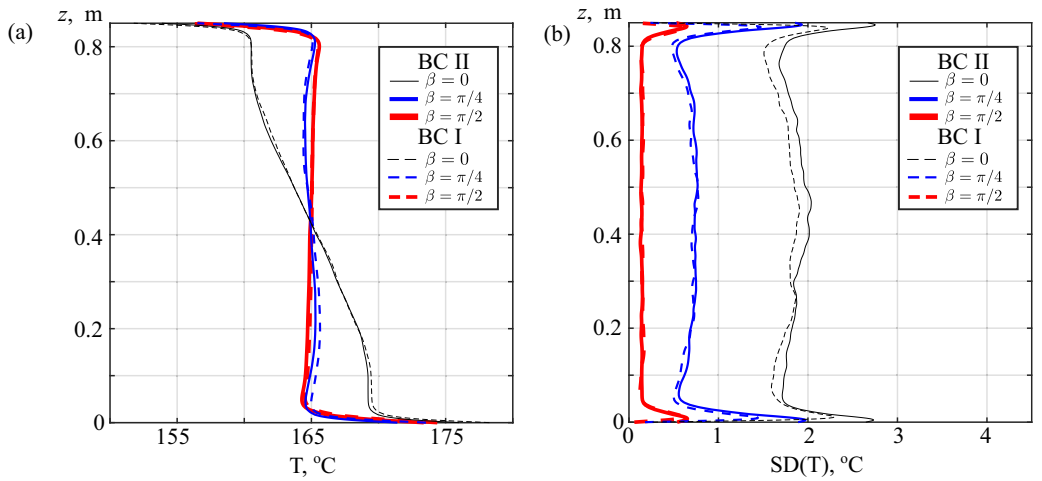

FIG. 8. (a) Time-averaged temperature and (b) its standard deviation along the cylinder axis for $\beta = 0$ (thin lines), $\beta = \pi/4$ (normal lines), and $\beta = \pi/2$ (thick lines). The results of simulations with BC II are shown by solid lines and simulations with BC I by dashed lines.

temperature and fixed heat flux BCs, we compare the temperature profiles. The averaged temperature and temperature SD along the axis of the cylinder are shown in Fig. 8. In the inclined and horizontal cylinders, the mean temperature along the axis is almost homogeneous. In the vertical cylinder, a linear temperature stratification is established in the bulk flow beyond two ring vortices near the faces. The most intense pulsations occur at $\beta = 0$ and the weakest pulsations exist at $\beta = \pi/2$. The profiles of the averaged temperature are practically not affected by the change of BC. The only difference concerns the pulsations in very thin boundary layers, for which BC I provides strong suppression of the temperature oscillations.

Figure 9 presents the averaged temperature and its SD along a line, parallel to the wall at a distance of 17 mm, where the thermocouples were installed in the experimental setup of [12]. Their

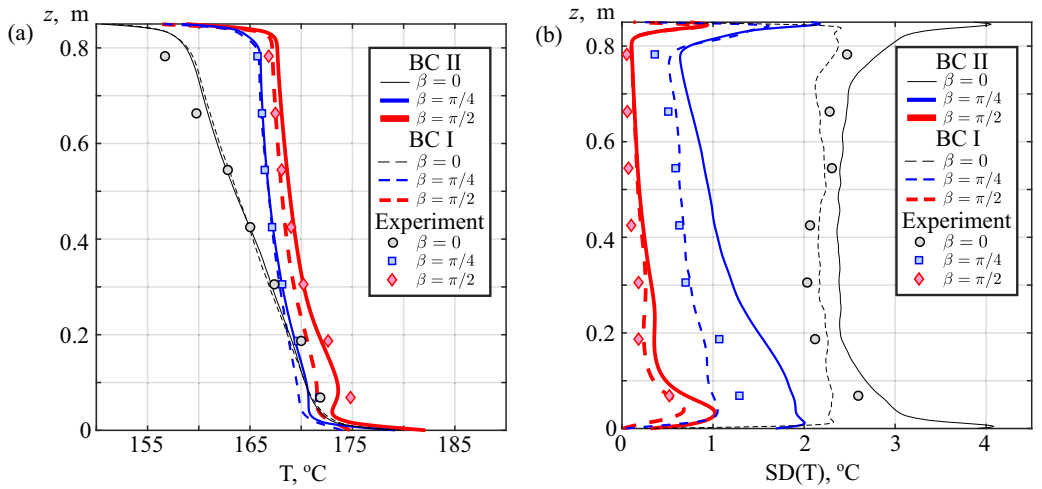

FIG. 9. (a) Time-averaged temperature and (b) its standard deviation along the line of probes for $\beta = 0$ (thin lines), $\beta = \pi/4$ (normal lines), and $\beta = \pi/2$ (thick lines). Experimental data of [12] are shown by large icons: circles for $\beta = 0$, squares for $\beta = \pi/4$, and diamonds for $\beta = \pi/2$. Results of simulations with BC II are shown by solid lines and simulations with BC I by dashed lines.

experimental points are also shown in this figure. For $\beta = 0$, the experimental points of the mean temperature in the upper part of the cylinder diverge from the numerical profiles (which follow a linear law in the bulk flow). The possible explanation is the construction of the cooling heat exchanger and the nonideal heat insulation of the walls in the experiments. Besides that, the agreement between experimental data and averaged temperature profiles is satisfactory, especially in the bulk flow [see Fig. 9(a)]. Figure 9(b) shows the corresponding SD profiles for the temperature. The temperature pulsations for BCs with fixed heat flux are always higher than in the experiment. In contrast, the temperature pulsations with fixed temperature BCs are lower and closer to the experimental data.

V. DEPENDENCE OF REYNOLDS AND NUSSELT NUMBERS ON THE INCLINATION ANGLE

The Reynolds and Nusselt numbers are the two main integral characteristics of convection, describing the intensity of convective flow and the effective axial heat transport. Figures 3 and 4 demonstrate that the main kinetic energy of convective flow can be associated with the large-scale mean flow ($\beta = \pi/2$) or with the small-scale turbulence ($\beta = 0$). Therefore, we divide the velocity into two parts $\mathbf{v} = \mathbf{U} + \mathbf{u}'$, the averaged velocity $\mathbf{U} = \langle \mathbf{v} \rangle_t$ and the velocity pulsation $\mathbf{u}' = \mathbf{v} - \mathbf{U}$, where $\langle \cdot \rangle_t$ denotes averaging over time. Then we define the total Reynolds number

$$\mathrm{Re}_{\mathrm{tot}} = \sqrt{\langle \mathbf{v} \cdot \mathbf{v} \rangle} D/\nu. \tag{1}$$

Here $\langle \cdot \rangle$ denotes averaging over time and over the whole convection cell and there are two additional numbers: The large-scale Re_U (a characteristic of the averaged flow) and small-scale Re_u (a characteristic of small-scale turbulence) are

$$\mathrm{Re}_U = \sqrt{\langle \mathbf{U} \cdot \mathbf{U} \rangle} D/\nu, \quad \mathrm{Re}_u = \sqrt{\langle \mathbf{u}' \cdot \mathbf{u}' \rangle} D/\nu. \tag{2}$$

The dependence of Reynolds numbers on inclination angle (under fixed heat flux) is shown in Fig. 10(a). The plot clearly illustrates the dynamics of convective flow in an inclined cylinder. The total Reynolds number slightly increases with the inclination of the cylinder from the vertical. It reaches the maximal value at $\beta \approx \pi/6$ and essentially decreases on approaching the horizontal position. The contributions of the large-scale and small-scale parts in the total Reynolds number are very different. The small-scale contribution dominates at small inclination angle. The corresponding Reynolds number Re_u is maximal in the vertical position and decreases monotonically with

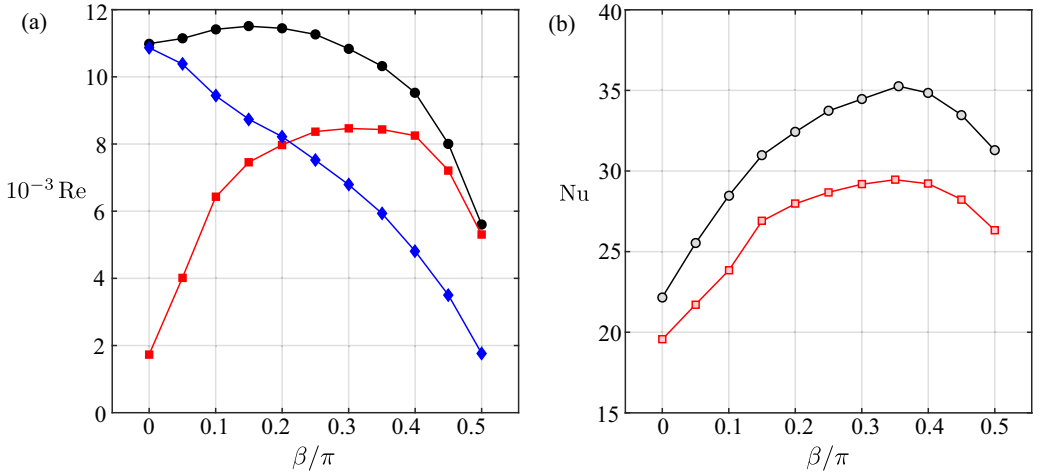

FIG. 10. (a) Reynolds numbers $\mathrm{Re}_{\mathrm{tot}}$ (circles), Re_U (squares), and Re_u (diamonds) versus the inclination angle β. (b) Nusselt number versus the inclination angle β showing the results of simulations with BC I (open squares) and BC II (open circles).

increasing β. The large-scale flow is negligible in the vertical cylinder. The averaged flow is weak and is concentrated near the faces [Fig. 3(a)]. Therefore, Re_U is low and strongly increases with β under weak inclination. Under moderate inclination, $\mathrm{Re}_U(\beta)$ possesses a flat maximum (at $\pi/4 \lesssim \beta \lesssim 2\pi/5$) and it steeply decreases on approaching $\beta = \pi/2$.

The Nusselt number for BC I is defined as

$$\mathrm{Nu} = \frac{\langle v_z T\rangle_z - \chi\,\partial_z\langle T\rangle_z}{\chi\,\Theta L^{-1}}, \tag{3}$$

where $\langle\cdot\rangle_z$ denotes averaging over any plane $z = \text{const}$ and over time and Θ is the applied fixed temperature difference between the faces. In simulations with BC II, the heat flux q is fixed and

$$\mathrm{Nu} = \frac{q}{\lambda\,\Theta_q L^{-1}}, \tag{4}$$

where λ is the thermal conductivity of sodium and Θ_q is the calculated difference of the average temperature over the heater and cooler plates under fixed heat flux q.

The dependence of the Nusselt number on inclination angle is shown in Fig. 10(b). The simulations were done for the inclination angle range $0 \leqslant \beta \leqslant \pi/2$ with a step $\pi/20$. Open circles in Fig. 10(b) show the results of simulations with fixed heat flux and open squares show the results of simulations with fixed face temperatures (e.g., BC I). The dependence of $\mathrm{Nu}(\beta)$ demonstrates similar behavior for both BCs, but the absolute values of the Nusselt number are smaller under BC I.

The lowest value of the Nusselt number is obtained at $\beta = 0$. Then, with increasing inclination angle, the efficiency of the heat transfer monotonically increases up to $\beta \approx 7\pi/20$. In that position, the value of Nu exceeds its value for the vertical cylinder by 51% under BC I and by 59% under BC II. On further increasing the inclination angle, the efficiency of the heat transfer decreases and for $\beta = \pi/2$, the value of Nu exceeds that for the vertical cylinder by 35% under BC I and by 41% under BC II.

Comparing two curves for $\mathrm{Nu}(\beta)$, we conclude that under fixed heat flux, convective heat transport is more efficient at any inclination angle. The reason is that the heat flux with a homogeneous temperature of the end faces is weaker in comparison with the heat flux with an inhomogeneous temperature distribution, which occurs for a face with an applied homogeneous heat flux with same averaged over the face temperature. In simulations with fixed heat flux the total heat power was $Q = 1314$ W. For fixed temperature BCs, the average heat flux through the liquid is smaller by 12% for $\beta = 0$, by 17% for $\beta = 7\pi/20$, and by 16% for $\beta = \pi/2$. Note that the dependence on the inclination angle is stronger under BC II. Under BC I, the maximum is flatter, though the position of the maximum is the same.

VI. DISCUSSION AND CONCLUSION

Numerical simulations of the turbulent convection of liquid sodium ($\mathrm{Pr} = 0.0083$) under Rayleigh numbers $\mathrm{Ra}_D \approx 6\times10^6$ in an inclined cylinder with aspect ratio $L = 5D$, heated at one end face and cooled at the other, showed that the structure of the flow strongly depends on the inclination angle. A stable LSC exists in the horizontal cylinder ($\beta = \pi/2$). This LSC is slightly disturbed by small-scale turbulence, which is weak (the energy of turbulent pulsations is about 10% of the energy of averaged flow). A deviation from the horizontal position provides a strong amplification of both LSC and small-scale turbulence. The energy of turbulent pulsations increases monotonically with decreasing inclination angle β, matching the energy of LSC at $\beta \approx \pi/5$. The intensity of LSC, characterized by the Reynolds number Re_U, has a wide, almost flat, maximum for an inclined cylinder, which slumps on approaching the horizontal and in particular the vertical position. In the last case ($\beta = 0$), the LSC vanishes. The dependence of the Nusselt number on the inclination angle has a maximum at $\beta \approx 7\pi/20$ and generally follows the dependence of the intensity of LSC on the inclination. This indicates that the total heat transport is highly determined by LSC.

TABLE I. Nusselt numbers (shown in bold) for three positions of the cylinder: $\beta = 0$, $\beta = \pi/4$, and $\beta = \pi/2$. We show the results of our numerical simulations with two types of BCs and experiments of [12] for the cylinder with the same aspect ratio $L = 5D$. In addition, we present Nusselt numbers obtained for the same inclinations in numerical simulations for a short cylinder in [9] and in laboratory experiments for a long cylinder in [14]. The normalized Nusselt number $\mathrm{Nu}(\beta)/\mathrm{Nu}(0)$ is given in parentheses.

	Numerical simulations				
Parameter	BC I	BC I	BC II	Experiments	
Pr	0.1	≈0.008 (Na)	≈0.008 (Na)	≈0.008 (Na)	≈0.008 (Na)
L	D	$5D$	$5D$	$5D$	$20D$
$\beta = 0$	**7.2** (1)	**19.6** (1)	**22.2** (1)	**28.6** (1)	**10** (1)
$\beta = \pi/4$	**8.5** (1.18)	**28.7** (1.47)	**33.7** (1.52)	**59.3** (2.1)	**80** (8)
$\beta = \pi/2$	**7.5** (1.04)	**26.3** (1.35)	**31.3** (1.41)	**39.7** (1.4)	**40** (4)
Reference	[9]	present work	present work	[12]	[14]

We have examined the applicability of idealized thermal BC for modeling real low-Prandtl-number flows. The simulations were done with two types of temperature BCs: BC II (Neumann, fixed heat flux) and BC I (Dirichlet, fixed temperature). The change of thermal BC does not affect the structure of the flow. The intensity of LSC is slightly higher under BC II versus BC I. This leads to a corresponding increase of convective heat flux and enhancement of temperature pulsations. The agreement between experimental data and averaged temperature profiles is satisfactory for both BC I and BC II simulations, but the temperature pulsations with BC I are closer to the experimental data. If a criterion for the correspondence of numerical and experimental results is defined, one can apply a combination of both BCs, i.e., boundary conditions of the third type (Robin BCs).

We show in Table I the Nusselt numbers for three inclination angles, obtained in simulations with different BCs together with the experimental data, obtained in an experiment with sodium in a cylinder with the same aspect ratio ($L = 5D$) under similar Rayleigh numbers [12]. A direct comparison of Rayleigh and Nusselt numbers in numerical and laboratory experiments is difficult, because an accurate determination of the temperature of the inner surfaces of the copper plates was impossible. To calculate Rayleigh and Nusselt numbers in experiment, the temperature difference measured by two thermocouples, installed on the axis of the cylinder in the vicinity of both end faces (about 4–5 mm), was used [12]. Therefore, the temperature difference was underestimated, which leads to an underestimation of the Rayleigh number and an overestimation of the Nusselt number. Experimental values of Nu are regularly higher than numerical values for the same inclination angle. To isolate the effect of inclination, we show in parentheses the Nusselt number, normalized by its value for the vertical position, i.e., $\mathrm{Nu}(\beta)/\mathrm{Nu}(0)$. Then the numerical value approaches the experimental one for horizontal cylinder but remains essentially lower (1.5 versus 2.1) for an inclined cylinder ($\beta = \pi/4$).

For a better understanding of the general tendency of turbulent convective flux transport for the cylinder aspect ratio and inclination angle, we show in Table I the Nusselt numbers obtained for the same three inclination angles from the numerical simulations for a short cylinder (first column) [9] and from the experiments in a long tube (last column) [14]. We emphasize that numerical values [9] were for a much *shorter* cylinder ($L = D$) and higher Prandtl number ($\mathrm{Pr} = 0.1$). The experiments [14] were done with liquid sodium in a much *longer* cylinder ($L = 20D$) for a similar applied temperature difference but a correspondingly large difference in the heat flux. Therefore, the comparison should be done with care. However, analyzing the table, we conclude that the dependence of convective heat transfer on the inclination becomes much stronger in long cylinders. Not only does the maximal value of $\mathrm{Nu}(\beta)/\mathrm{Nu}(0)$ increase, but this maximum in long cylinders becomes more narrow [compare Fig. 4 in Ref. [9], Fig. 10(b) in the present paper, and Fig. 3 in Ref. [14]). The location of the maximum is similar in all cases.

ACKNOWLEDGMENT

This work was supported by the Russian Foundation for Basic Research under Project No. 16-01-00459.

[1] B. Castaing, G. Gunaratne, L. Kadanoff, A. Libchaber, and F. Heslot, Scaling of hard thermal turbulence in Rayleigh-Bénard convection, J. Fluid Mech. **204**, 1 (1989).

[2] S. Grossmann and D. Lohse, Scaling in thermal convection: A unifying theory, J. Fluid Mech. **407**, 27 (2000).

[3] G. Ahlers, S. Grossmann, and D. Lohse, Heat transfer and large scale dynamics in turbulent Rayleigh-Bénard convection, Rev. Mod. Phys. **81**, 503 (2009).

[4] F. Chilla and J. Schumacher, New perspectives in turbulent Rayleigh-Bénard convection, Eur. Phys. J. E **35**, 58 (2012).

[5] F. Chillá, M. Rastello, S. Chaumat, and B. Castaing, Long relaxation times and tilt sensitivity in Rayleigh Bénard turbulence, Eur. Phys. J. B **40**, 223 (2004).

[6] C. Sun, H.-D. Xi, and K.-Q. Xia, Azimuthal Symmetry, Flow Dynamics, and Heat Transport in Turbulent Thermal Convection in a Cylinder with an Aspect Ratio of 0.5, Phys. Rev. Lett. **95**, 074502 (2005).

[7] G. Ahlers, E. Brown, and A. Nikolaenko, The search for slow transients, and the effect of imperfect vertical alignment, in turbulent Rayleigh-Bénard convection, J. Fluid Mech. **557**, 347 (2006).

[8] S. Weiss and G. Ahlers, Effect of tilting on turbulent convection: Cylindrical samples with aspect ratio, J. Fluid Mech. **715**, 314 (2013).

[9] O. Shishkina and S. Horn, Thermal convection in inclined cylindrical containers, J. Fluid Mech. **790**, R3 (2016).

[10] R. Langebach and Ch. Haberstroh, Natural convection in inclined pipes - A new correlation for heat transfer estimations, in *Advances in Cryogenic Engineering: Transactions of the Cryogenic Engineering Conference - CEC*, edited by J. G. Weisend II *et al.*, AIP Conf. Proc. No. 1573 (AIP, Melville, 2014), pp. 1504–1511.

[11] X. Riedinger, J.-C. Tisserand, F. Seychelles, B. Castaing, and F. Chillà, Heat transport regimes in an inclined channel, Phys. Fluids **25**, 015117 (2013).

[12] P. Frick, R. Khalilov, I. Kolesnichenko, A. Mamykin, V. Pakholkov, A. Pavlinov, and S. Rogozhkin, Turbulent convective heat transfer in a long cylinder with liquid sodium, Europhys. Lett. **109**, 14002 (2015).

[13] A. Mamykin, P. Frick, R. Khalilov, I. Kolesnichenko, V. Pakholkov, S. Rogozhkin, and A. Vasiliev, Turbulent convective heat transfer in an inclined tube with liquid sodium, Magnetohydrodynamics **51**, 329 (2015).

[14] A. Y. Vasil'ev, I. V. Kolesnichenko, A. D. Mamykin, P. G. Frick, R. I. Khalilov, S. A. Rogozhkin, and V. V. Pakholkov, Turbulent convective heat transfer in an inclined tube filled with sodium, J. Tech. Phys. **60**, 1305 (2015).

[15] F. H. Busse, On Howard's upper bound for heat transport by turbulent convection, J. Fluid Mech. **37**, 457 (1969).

[16] J. Schumacher, V. Bandaru, A. Pandey, and J. D. Scheel, Transitional boundary layers in low-Prandtl-number convection, Phys. Rev. Fluids **1**, 084402 (2016).

[17] J. D. Scheel and J. Schumacher, Global and local statistics in turbulent convection at low Prandtl numbers, J. Fluid Mech. **802**, 147 (2016).

[18] I. V. Kolesnichenko, A. D. Mamykin, A. M. Pavlinov, V. V. Pakholkov, S. A. Rogozhkin, P. G. Frick, R. I. Khalilov, and S. F. Shepelev, Experimental study on free convection of sodium in a long cylinder, Therm. Eng. **62**, 414 (2015).

[19] J. Smagorinsky, General circulation experiments with the primitive equations, Mon. Weather Rev. **91**, 99 (1963).

[20] J. W. Deardorff, A numerical study of three-dimensional turbulent channel flow at large Reynolds numbers, J. Fluid Mech. **41**, 453 (1970).
[21] R. Verzicco and R. Camussi, Numerical experiments on strongly turbulent thermal convection in a slender cylindrical cell, J. Fluid Mech. **477**, 19 (2003).
[22] R. J. A. M. Stevens, R. Verzicco, and D. Lohse, Radial boundary layer structure and Nusselt number in Rayleigh-Bénard convection, J. Fluid Mech. **643**, 495 (2010).
[23] O. Shishkina, R. J. A. M. Stevens, S. Grossmann, and D. Lohse, Boundary layer structure in turbulent thermal convection and its consequences for the required numerical resolution, New J. Phys. **12**, 075022 (2010).
[24] H. K. Versteeg and W. Malalasekera, *An Introduction to Computational Fluid Dynamics: The Finite Volume Method* (Pearson Education, Harlow, 2007).
[25] H. G. Weller, G. Tabor, H. Jasak, and C. Fureby, A tensorial approach to computational continuum mechanics using object-oriented techniques, Comput. Phys. **12**, 620 (1998).
[26] H. Johnston and C. R. Doering, Comparison of Turbulent Thermal Convection Between Conditions of Constant Temperature and Constant Flux, Phys. Rev. Lett. **102**, 064501 (2009).
[27] R. Verzicco and K. R. Sreenivasan, A comparison of turbulent thermal convection between conditions of constant temperature and constant heat flux, J. Fluid Mech. **595**, 203 (2008).